Turbulence statistics in Couette flow at high Reynolds number

SERGIO PIROZZOLI, MATTEO BERNARDINI and PAOLO ORLANDI

Dipartimento di Ingegneria Meccanica e Aerospaziale, Università di Roma 'La Sapienza'
Via Eudossiana 18, 00184 Roma, Italy

(Received 8 September 2014)

We investigate the behavior of the canonical turbulent Couette flow at computationally high Reynolds number through a series of large-scale direct numerical simulations (DNS). We achieve a Reynolds number $Re_\tau = h/\delta_v \approx 1000$, where h is the channel half-height, and δ_v is the viscous length scale) at which some phenomena representative of the asymptotic Reynolds number regime manifest themselves. While a logarithmic mean velocity profile is found to provide a reasonable fit of the data, including the skin friction, closer scrutiny shows that deviations from the log law are systematic, and probably increasing at the higher Reynolds numbers.

The Reynolds stress distribution shows the formation of a secondary outer peak in the streamwise velocity variance, which is associated with significant excess of turbulent production as compared to the local dissipation. This excess is related to the formation of large-scale streaks/rollers, which are responsible for a substantial fraction of the turbulent shear stress in the channel core, and for significant increase of the turbulence intermittency in the near-wall region.

1. Introduction

Turbulent Couette flow, which is physically realized by differential motion of two parallel infinite flat plates, is probably the most prototypical among canonical wall-bounded flows, being homogeneous in two space directions, and having no imposed mean pressure gradient. Hence, it is the only flow to experience exactly constant total stress across the thickness, which is one of the hypothesis requested by Prandtl's classical arguments for the existence of a logarithmic layer. Because of its (apparent) simplicity, Couette flow is frequently taken as an illustrative example for the structure of turbulent wall-bounded flows in classical books (Schlichting & Gersten 2000), and it has been the subject of several theoretical investigations, aimed at clarifying the mechanisms responsible for the self-sustainment of near-wall turbulence (Hamilton *et al.* 1995; Waleffe 1997), and for the onset of outer-layer energy-containing modes (Hwang & Cossu 2010). Also, because of the establishment of strong large-scale outer-scaled motions, Couette flow is an ideal testbed for probing inner-outer wall turbulence interaction phenomena of imprinting and modulation (Pirozzoli *et al.* 2011).

Despite its apparent simplicity, Couette flow poses significant challenges to experimental investigations, typically carried out by means of moving belts which are prone to deform, especially at high speed. As a consequence, pure Couette flow has received much less attention as compared to, e.g. Poiseuille pressure flow in channels and pipes. Relevant early studies include those of Reichardt (1956); Robertson (1959); El Telbany

& Reynolds (1982); Aydin & Leutheusser (1991); Tillmark & Alfredsson (1992), which are all limited to $Re_c \lesssim 20000$, where $Re_c = u_c h/\nu$ is the Reynolds number based on the half velocity difference between the two walls (u_c), and the channel half-height (h). Experiments have allowed to clarify some peculiar features of Couette flow, namely the onset of large-scale motions in the form of rolls/streaks pairs, which occupy the whole channel, and whose typical streamwise and spanwise wavelengths are $\lambda_x = 40 - 65h$, $\lambda_z = 4 - 5h$, respectively (Tillmark & Alfredsson 1998; Kitoh *et al.* 2005). However, as also apparent in recent studies (Kitoh & Umeki 2008), there is very little consensus among different experimental set-ups, even for global quantities such as skin friction. Over the years, the origin of the formation and sustainment of the h-scaled rolls has been traced to mechanisms of nonlinear feedback caused by streaks instability (Hamilton *et al.* 1995), or to transient growth phenomena (Hwang & Cossu 2010).

Given the difficulties encountered by experiments, DNS constitutes an invaluable tool for the study of turbulence in Couette flow. Indeed, early numerical experiments (Lee & Kim 1991; Bech *et al.* 1995) confirmed the existence of large-scale structures which qualitatively resemble those observed in experiments. However, it soon became clear that the size and the persistence of those large eddies poses stringent demand to DNS in terms of the size of the computational box, which shall be large enough to contain at least a representative ensemble of them. Detailed studies in this respect (Komminaho *et al.* 1996; Tsukahara *et al.* 2006) have shown that, in order to alleviate spurious effects of flow confinement, boxes with size $L_x \approx 60h$, $L_z \approx 16h$ are needed. Since the size of the h-scaled eddies is not expected to depend significantly on the Reynolds number (the effect of viscosity being mainly concentrated in the thin near-wall sublayer), and since the mesh resolution for DNS should stay constant in wall units, it follows that the total number of grid points should roughly grow as Re_τ^3, a more accurate estimate being $Re_\tau^{11/4}$ (Pope 2000). It is then clear that huge computational resources are required even at moderate Reynolds numbers. For this reason, the upper limit of Reynolds number achieved so far in DNS is $Re_c \approx 3000$ (Lee & Kim 1991), corresponding to friction Reynolds number $Re_\tau \approx 170$ (here $Re_\tau = hu_\tau/\nu$, where $u_\tau = \sqrt{\tau_w/\rho}$ is the friction velocity), although in rather narrow computational box, having length $4\pi h$ and width $8/3\pi h$. Therefore, in this respect it is more relevant to cite the study of Tsukahara *et al.* (2006), in which $Re_\tau \approx 130$ was achieved in large computational boxes. Results of Couette flow at Re_τ up to 550 in wide boxes have recently been presented by Avsarkisov *et al.* (2014).

The main goal of this paper is to widen the Reynolds number envelope for turbulent Couette flow, thus analysing physical phenomena not accessible so far. A special effort will be made to clarify the reasons for the observed deviations from a 'canonical' behavior, and to highlight the contribution of the large-scale motions to the overall dynamics.

2. Computational setup

We solve the Navier-Stokes equations for a divergence-free velocity field, which are discretized in an orthogonal coordinate system (x, y, z denote the streamwise, wall-normal and spanwise directions) using staggered central second-order finite-difference approximations, so as to guarantee that kinetic energy is globally conserved in the limit of inviscid flow. Time advancement is carried out by means of a hybrid third-order low-storage Runge-Kutta algorithm, coupled with the second-order Crank-Nicolson scheme, combined in the fractional-step procedure, whereby the convective and the diffusive terms are treated explicitly and implicitly, respectively. The Poisson equation for the pressure field, stemming from the incompressibility condition, is efficiently solved through Fourier

Flow case	Line style	Re_c	Re_τ	N_x	N_y	N_z	Δx^+	Δz^+	Tu_τ/h
C1	Dashed	3000	171	1280	256	896	7.55	4.80	113.9
C2	Dash-dot	4800	260	2048	256	1280	7.18	5.10	72.2
C3	Dash-dot-dot	10133	507	4096	384	2560	7.00	4.99	74.9
C4	Solid	21333	986	8192	512	5120	6.80	4.84	54.1

Table 1: List of parameters for turbulent Couette flow cases. $Re_c = hu_c/\nu$ is the bulk Reynolds number, and $Re_\tau = hu_\tau/\nu$ is the friction Reynolds number, with u_c the centerline velocity. N_x, N_y, N_z are the number of grid points in the streamwise, wall-normal, and spanwise directions. Δx^+, Δz^+ are the grid spacings in the wall-parallel direction, in wall units. The time window used for collecting the flow statistics T is given in terms of eddy turnover times h/u_τ.

transform-based methods (Kim & Moin 1985). A full description of the numerical method is provided in Orlandi (2000).

For the sake of convenience (Bernardini *et al.* 2013) the computations are carried out in a reference frame in which the bulk velocity is zero, hence the lower wall moves at a speed $-u_c$, and the upper wall with a speed $+u_c$. The DNS have been carried out in a $(L_x \times L_y \times L_z) = (18\pi h \times 2h \times 8\pi h)$ computational box, which based on previous experiences (Komminaho *et al.* 1996; Tsukahara *et al.* 2006) at much lower Reynolds number is expected to be sufficient to prevent spurious dynamics from developing. Hereinafter, the nondimensional wall-normal coordinate η will be used, in such a way that $\eta = 0$ corresponds to the channel centerline, and $\eta = \pm 1$ corresponds to the two walls, whereas the distance from the nearest wall will be denoted with y. The mesh spacing in the wall-parallel directions has been kept approximately the same in wall units for all the simulations, accounting for grid refinement tests carried out in previous studies (Bernardini *et al.* 2014). An error-function mapping ($\eta(\xi) = \mathrm{erf}(\alpha\xi/2)/\mathrm{erf}(\alpha/2)$, $\xi = [-1; 1]$, with $\alpha = 4$) has been used to cluster points in the wall-normal direction, in such a way that the first point off the wall is at $\Delta y_w^+ \leqslant 0.08$. Details on the computational mesh and on the flow parameters for the DNS are provided in table 1.

The simulations have been initiated with a linear velocity profile, with superposed random disturbances. After the initial transient, spatial averages of the flow fields in wall-parallel planes are collected at time intervals of $\Delta t \approx h/u_c$. The time window used for the averaging procedure (see table 1) was selected by monitoring the running averages of the velocity variances at the channel centerline. In the worst case, the running average of the streamwise velocity variance ranges within a band of no more that 1% with respect to its final value. A validation study of the solver for Couette flow is reported in Pirozzoli *et al.* (2011), and not repeated here.

As frequently quoted in the literature (Komminaho *et al.* 1996; Tsukahara *et al.* 2006), numerical simulations of plane Couette flow using periodic boundary conditions in the streamwise and in the spanwise direction tend to be significantly affected by the size of the computational box, which may yield unnatural confinement effects. This effect is monitored through the two-point correlation of the streamwise velocity fluctuations (R_{uu}), which is shown in figure 1, at the channel centerline. Regarding the streamwise direction (panel (a)), similar conclusions can be drawn as by Tsukahara *et al.* (2006),

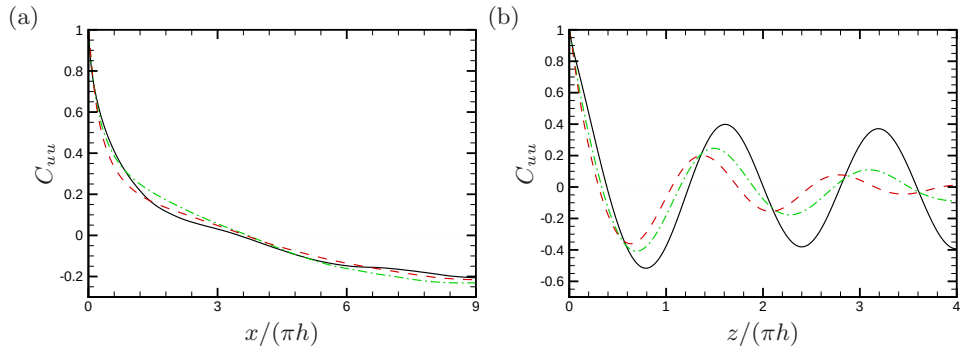

Figure 1: Streamwise (a) and spanwise (b) two-point correlation coefficient (R_{uu}) of streamwise velocity fluctuations at the channel centerline. See table 1 for nomenclature of the DNS data.

in that the box size is at least sufficient to have inversion in the sign of the correlation coefficient, which means that at least one streamwise wavelength is captured within the computational box. Contrary to the observations of Tsukahara *et al.* (2006), we do not note significant Reynolds number dependence for these statistics. The correlation coefficients in the spanwise direction are shown in figure 1(b). Results very similar as Tsukahara *et al.* (2006) are found at the lower Reynolds numbers (flow cases C1, C2), with the correlation decaying sufficiently fast away from the origin. However, at higher Reynolds numbers the first negative peak, which yields a typical spanwise size of the large-scale motions developing in the channel core, shifts to higher values, and the correlation does not drop off to zero at the maximum separation. This observation can be interpreted with the emergence of large-scale streaks/rollers in the core flow, which become stronger as the Reynolds number is increased. As discussed later, these streaks/rollers have a typical spanwise size of about $5h$, and they have a nearly sinusoidal dependence on the spanwise coordinate. Hence, their correlation length scale is nominally infinite. This implies that any simulation with finite spanwise extent is contaminated by confinement effects, and the case is also likely to be in experiments. The results shown in the following (and probably all experimental and numerical results for Couette flow) should then be interpreted with this caveat in mind.

3. Results

3.1. *Velocity statistics*

The mean streamwise velocity profiles for the C1-4 simulations are shown in figure 2(a), which well highlights the onset of a layer with nearly logarithmic velocity variation, whose width apparently increases with Re_τ. Visually fitting the Couette data with a logarithmic velocity distribution $\overline{u}^+ = 1/k \log y^+ + C$ suggests that the classical set of log-law coefficients $k \approx 0.41$, $C \approx 5$, adequately reproduces the DNS data. More refined information on the behavior of the mean velocity profile can be gained from inspection of the log-law diagnostic function

$$\Xi = y^+ \, \mathrm{d}\overline{u}^+/\mathrm{d}y^+, \tag{3.1}$$

shown in figure 2(b), whose constancy would imply the presence of a genuine logarithmic layer in the mean velocity profile. The figure supports universality of the mean velocity in inner units, with a near-wall maximum of about 5.5, which is nearly identical as in Poiseuille flow (Bernardini *et al.* 2014), followed by a minimum at $y^+ \approx 60$. Further away

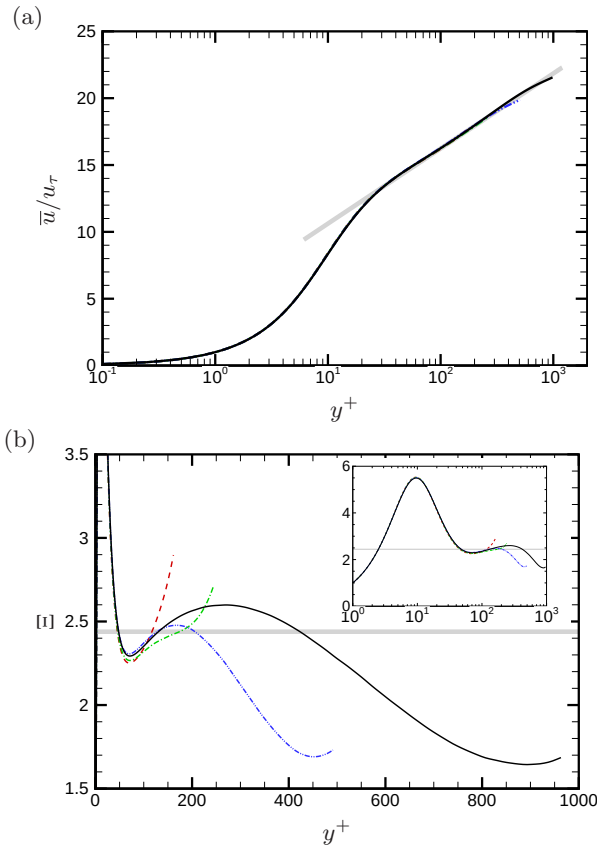

Figure 2: Distribution of mean velocity (a) and log-law diagnostic function (b), as defined in equation (3.1). The thick grey line correspond to the inner-layer log law, with $k = 0.41$, $C = 5$. The inset in panel (b) shows the same data on a semi-log diagram, to highlight the inner-layer peak. See table 1 for nomenclature of the DNS data.

from the wall, a maximum forms whose position scales in outer units, at $y/h \approx 0.25$. Between the two extrema the diagnostic function is far from constant, with a peak-to-peak difference which seems to even increase with Re_τ. Hence, based on the present results, asymptotic convergence of the mean velocity profile to the log law in the turbulent Couette flow is far from clear. This behavior is distinctly different than Poiseuille flow. In that case, recent DNS data (Bernardini *et al.* 2014) have shown the presence of systematic linear corrections to the log law, whose amplitude decreases as $1/Re_\tau$. Hence, in that case, logarithmic behavior should then be recovered in the infinite Re_τ limit. Possible alternatives to the logarithmic law have also been pursued, by monitoring the power-law diagnostic function, namely $y^+/\overline{u}^+(\mathrm{d}\overline{u}^+/\mathrm{d}y^+)$, whose constancy would imply power-law variation of the mean velocity. The resulting distributions, not shown, again do not show any significant plateau.

Mean velocity profiles in outer representation are shown in figure 3, where the streamwise velocity is normalized by either the wall speed, or by the friction velocity. The distinctive S-shaped profile typical of Couette flow is recovered in all cases. Notably, the slope of the profiles at the centerline seems to decrease in both representations, even though the decline is slower if the friction velocity is used for normalization. This ob-

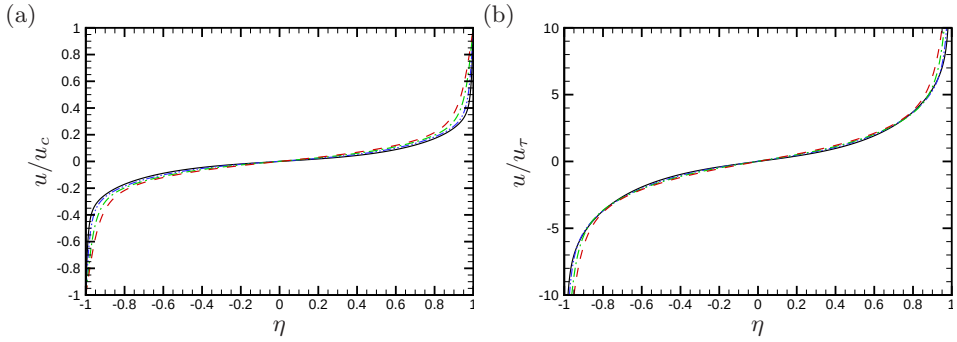

Figure 3: Mean velocity profiles scaled with u_c (a) and with u_τ (b). See table 1 for nomenclature of the DNS data.

servation has some interesting theoretical impact, as it relates to the asymptotic shape of the velocity profile in the $Re_\tau \to \infty$ limit. In this respect, several (often conflicting) statements have been made. According to some studies, the centerline velocity slope in outer units, $S = h/u_c(\mathrm{d}\overline{u}/\mathrm{d}y)$, should asymptote to a constant, typically quoted to be $S \approx 0.2$ (Busse 1970), whereas according to other the inner-scaled velocity slope $R_s = h/u_\tau(\mathrm{d}\overline{u}/\mathrm{d}y)$ should approach a limit value (Townsend 1976). However, none of the two scenarios has received any convincing support either in DNS or experiments (Kitoh *et al.* 2005), and different authors report different trends with Re. This is probably a consequence of experimental difficulties in measuring small velocity differences in internal flows. The slope parameters from the present DNS are shown in figure 4, as a function of Re_c, with additional data from earlier studies. Overall, we find substantial decrease of S, but we also notice slight decline of R_s. This observation seems to suggest that the defect law $u(y)/u_\tau = g(\eta)$ is not fully established (at least in this Reynolds number range), and thus the correct outer velocity scale is not simply u_τ. The issue of whether the inner slope parameter R_s attains a constant value cannot be sorted out based on the present data. Nevertheless, either if the decreasing trend continues or an asymptote is reached, it appears that the asymptotic core profile of Couette flow shall be flat in inner units (and in outer units as well), since $u_c/u_\tau \to \infty$ as $Re_\tau \to \infty$, and all the velocity difference is eventually supported in infinitely thin viscous layers adjacent to the walls.

Strictly related to the behavior of the mean velocity profile is the friction law. Most studies of Couette flow refer to empirical approximations for the friction law, as that given by Robertson (1959),

$$C_f = \frac{G}{\log Re_c^2}, \tag{3.2}$$

where $C_f = 2\tau_w/(\rho u_c^2)$, and various choices for the constant have been proposed, including $G = 0.383$ (Robertson 1959), $G = 0.351$ (El Telbany & Reynolds 1982), $G = 0.420$ (Tsukahara *et al.* 2006), $G = 0.382$ (Kitoh *et al.* 2005). Using the log-law representation of the mean velocity profile the following friction law is obtained (Schlichting & Gersten 2000)

$$\sqrt{\frac{2}{C_f}} = \frac{1}{k}\log\left(Re_c\sqrt{\frac{C_f}{2}}\right) + C + \overline{C}, \tag{3.3}$$

where $\overline{C}$ depends on the deviation of the core velocity profile from the log law. In figure 5 we show the present DNS data together with experimental data from several sources,

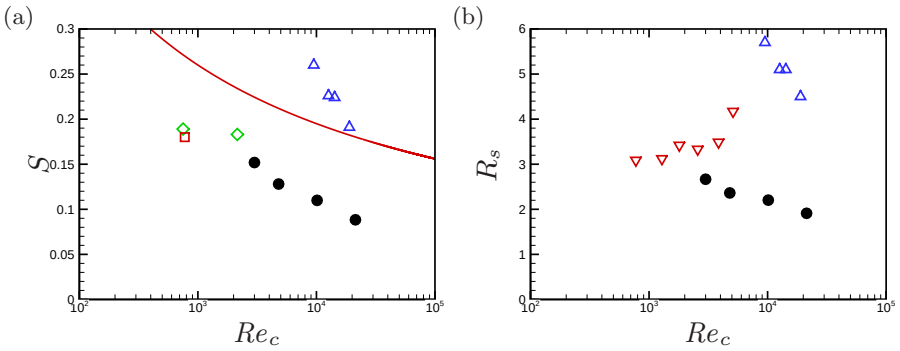

Figure 4: Mean velocity slope at centerline, scaled with u_c/h (a) and with u_τ/h (b), as a function of Reynolds number. The solid circles denote the present DNS data. The open symbols denote experimental data from Komminaho *et al.* (1996) (squares); Tsukahara *et al.* (2006) (diamonds); El Telbany & Reynolds (1982) (up-triangles); Kitoh *et al.* (2005) (down-triangles) The solid line denotes the fit $S = 0.34/\log_{10} Re_c$ (Robertson 1959).

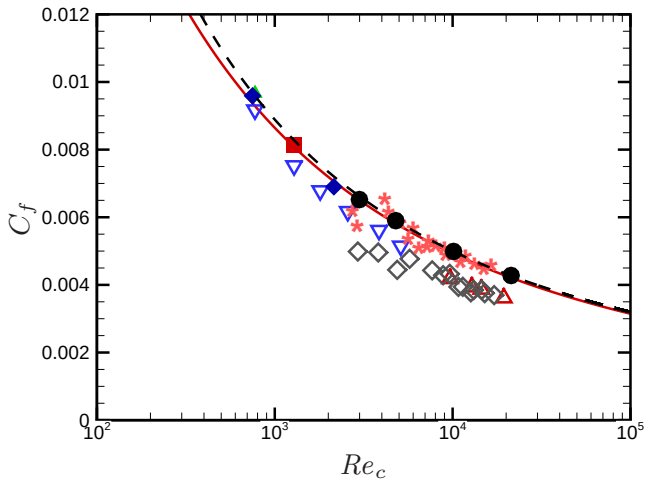

Figure 5: Comparison of skin friction coefficient with correlations and experiments. The solid circles denote DNS from the C1-4 datasets. Filled symbols refer to previous DNS data by Bech *et al.* (1995) (squares); Komminaho *et al.* (1996) (triangles); Tsukahara *et al.* (2006) (diamonds). Open symbols refer to experimental data by El Telbany & Reynolds (1982) (up-triangles); Kitoh *et al.* (2005) (down-triangles); Reichardt (1956) (diamonds); Robertson (1959) (stars). The solid line indicates the logarithmic friction law (3.3) with $k = 0.41$, $C = 5$, $\overline{C} = 0$; the dashed line indicates the friction law (3.2) with $G = 0.424$.

compared with formulas (3.2),(3.3). It appears that our data are consistent with previous DNS data at lower Reynolds number, altough they seem to be out of trend with respect to most experimental data (differences with respect to El Telbany & Reynolds (1982) are up to 20%), except for those of Reichardt (1956). Furthermore, our DNS data appear to be well consistent with the logarithmic friction law, by selecting $k \approx 0.41$, $C \approx 5$, $\overline{C} = 0$ (see figure 2), at least for $Re_c \gtrsim 10^3$, sufficient to observe a sensible near-logarithmic layer. The power-law fit (3.2) also appears to deliver adequate representation of the DNS data, by setting $G = 0.424$.

The second-order velocity fluctuations statistics are shown in inner coordinates in

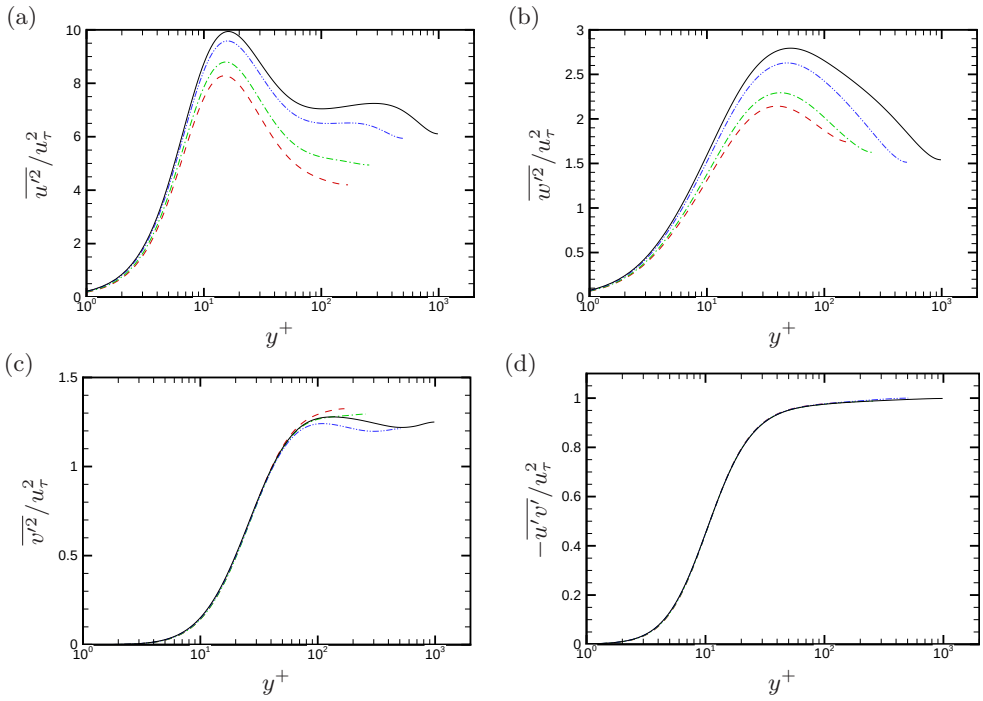

Figure 6: Distribution of Reynolds stress components across the channel in wall units. Refer to table 1 for nomenclature of the DNS data.

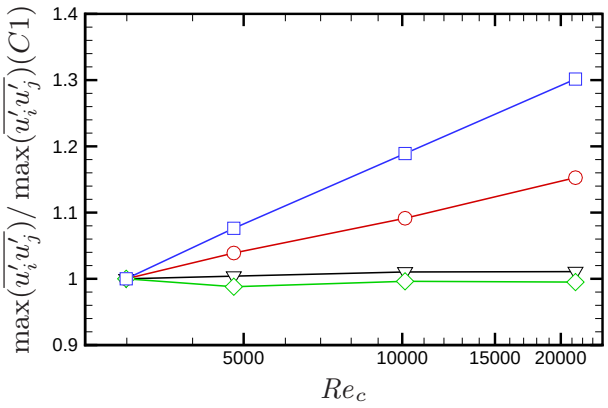

Figure 7: Peak Reynolds stress components as a function of Re_c, normalized by their value for the C1 flow case. Symbols: $i = j = 1$, circles; $i = j = 2$, diamonds; $i = j = 3$, squares; $i = 1, j = 2$, triangles.

figure 6, and their peaks reported in figure 7 as a function of Re_c. The main impression gained from the figures is that the trends observed in Poiseuille flow (Hoyas & Jiménez 2006; Bernardini *et al.* 2014) continue to hold. Specifically, the longitudinal (a) and the transverse (b) normal stresses show clear lack of universality, and their amplitudes increase nearly logarithmically with Re_τ. This behavior has been attributed (Metzger & Klewicki 2001; del Álamo *et al.* 2004; Mathis *et al.* 2009) to the increasing influence of inactive outer-layer modes. It is noteworthy that in the C4 flow case the Reynolds

number is high enough that a secondary outer peak of $\overline{u'^2}$ appears around $y^+ \approx 300$ ($y/h \approx 0.33$). The existence of a secondary peak of the streamwise velocity variance has been the subject of significant disputes in recent years (Hultmark *et al.* 2012), and it has sometimes been attributed to limited probe resolution effects in experiments. Alfredsson *et al.* (2011, 2012) proposed that in pipes, channel flows, and boundary layers, a secondary peak in $\overline{u'^2}$ should arise at $Re_\tau \gtrsim 15000$, thus explaining why it has not been observed in recent plane channel flow DNS at $Re_\tau \approx 4000$ (Bernardini *et al.* 2014). Those authors noticed that the position of the outer peak scales as $Re_\tau^{1/2}$, hence it is proportional to the position of the turbulent shear stress peak. As a consequence, the secondary peak should rather be interpreted as a second inner peak than a real outer peak. The nature of the secondary peak here observed for Couette flow is probably different than in other canonical wall-bounded flows, occurring much earlier in term of Reynolds number, and residing at much larger distance from the wall.

The wall-normal velocity fluctuations and the turbulent shear stress (see panels (c),(d)) exhibit near-universality in inner scaling. This behavior is entirely consistent with Townsend's attached-eddy hypothesis (Townsend 1976), however, it is somewhat different from the case of Poiseuille flow, in which the wall-normal stress exhibits slow but consistent growth with Re_τ (Bernardini *et al.* 2014), consistent with the continuing growth of the peak turbulent shear stress.

3.2. *Velocity spectra*

The emergence of an outer peak of the streamwise Reynolds stress can be well understood by monitoring the pre-multiplied spectral densities of u, shown in figure 8. The figure highlights the presence of a main energetic inner-layer site at $y^+ \approx 15$, corresponding to inner-layer streaks with a typical wavelength of about 100 wall units, which is roughly universal across the Reynolds number range, for all wall-bounded flows (Monty *et al.* 2009). Similar to other canonical flows, the spectra also exhibit a secondary energetic site in the outer layer, whose intensity increases in wall units, and which has been traditionally associated with boundary layer superstructures (Hutchins & Marusic 2007), and large-scale and very-large-scale motions in internal flows (Hoyas & Jiménez 2006; Kim & Adrian 1999). In the case of the Couette flow we find that the spectral footprint of these organized structures consists of a nearly pure tone at the wavelength $\lambda_z \approx 5h$, with a weaker secondary harmonic spectral line visible in the C3 and C4 flow cases. The intensity of the outer peak appears to be much higher than in other wall-bounded flows at the same Reynolds number. Apparently, the effect of the peak is felt all the way down to the wall, especially at the higher Reynolds numbers. It is noteworthy that the spectral signature in the core part of the flow is consistent with simple inviscid models of rollers (Waleffe 1997; Papavassiliou & Hanratty 1997), which predict $u(y,z) \sim \cos(\pi/2\eta)\cos(\beta z)$, where $\beta = 2\pi/\lambda_z$ is the roll wavenumber in the spanwise direction.

The observed structural flow changes with Re_τ can be interpreted by monitoring the local excess of kinetic energy production ($P = -(\mathrm{d}\overline{u}/\mathrm{d}y)\overline{u'v'}$) over its dissipation rate ($\varepsilon = 2\nu\overline{s'_{ij}s'_{ij}}$). This is shown in figure 9, where we report the distributions of $P-\varepsilon$ in pre-multiplied form, so that equal areas underneath the curves correspond to equal integral contributions. Figure 9 confirms the presence of a strong excess of production centered at $y^+ \approx 15$, which corresponds to the near-wall turbulence self-sustainment cycle, and which is universal in wall units. However, the figure also shows the onset of a secondary spot with excess production, whose position moves outwards in wall units. Notably, in the C4 flow case, the peak location coincides with the position of the secondary peak of the streamwise velocity variance (see figure 6a). At the highest Reynolds number achieved in the present study, that peak accounts for an integrated production excess which is

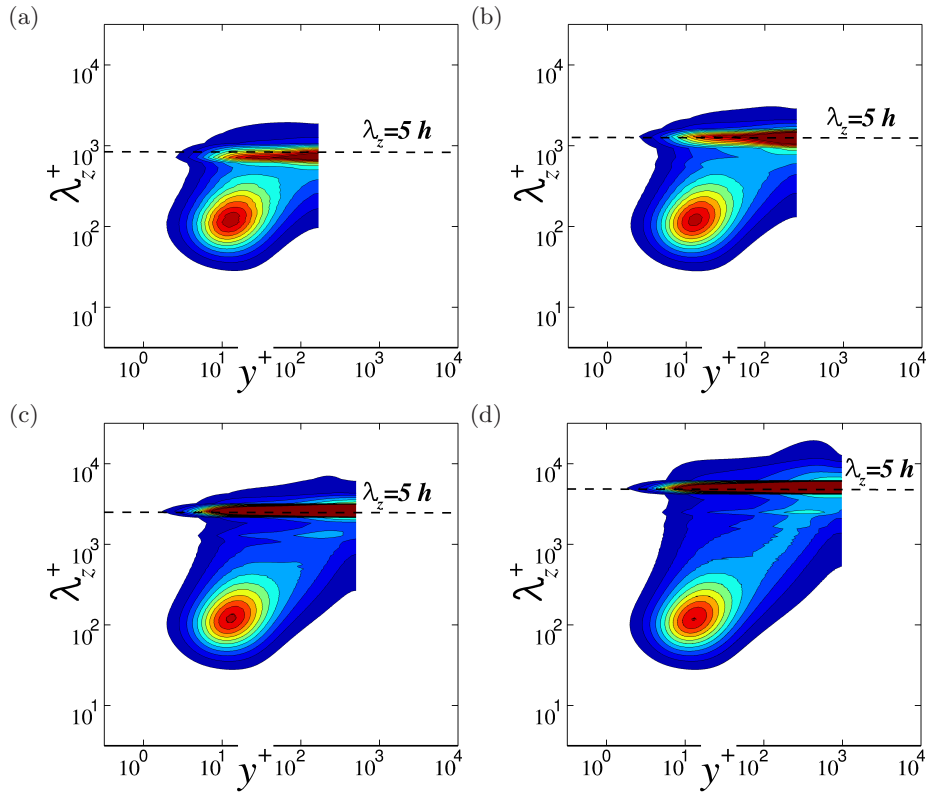

Figure 8: Variation of pre-multiplied spanwise spectral density of u ($k_z E_{uu}/u_\tau^2$) with wall distance, for flow cases C1 (a), C2 (b), C3 (c), C4 (d). Twelve contour levels are shown, from 0.32 to 3.8.

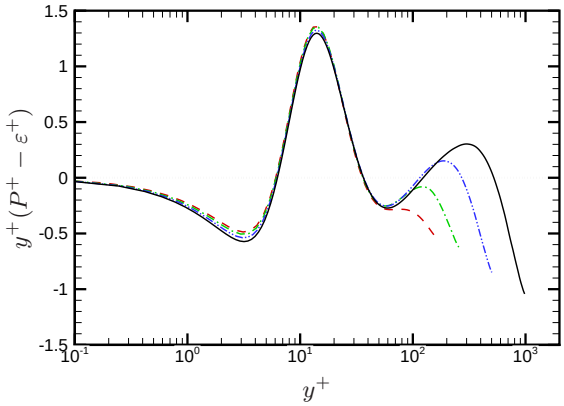

Figure 9: Distribution of pre-multiplied turbulence kinetic energy production excess. See table 1 for nomenclature of the DNS data.

about 20% as the inner production site. Hence, its effect on the overall wall dynamics is certainly not negligible, and it is observed to increase with Re_τ. A similar (even though much less evident) effect has also been observed in Poiseuille flow (Hoyas & Jiménez 2008; Bernardini *et al.* 2014). The presence of the outer peak implies that the excess

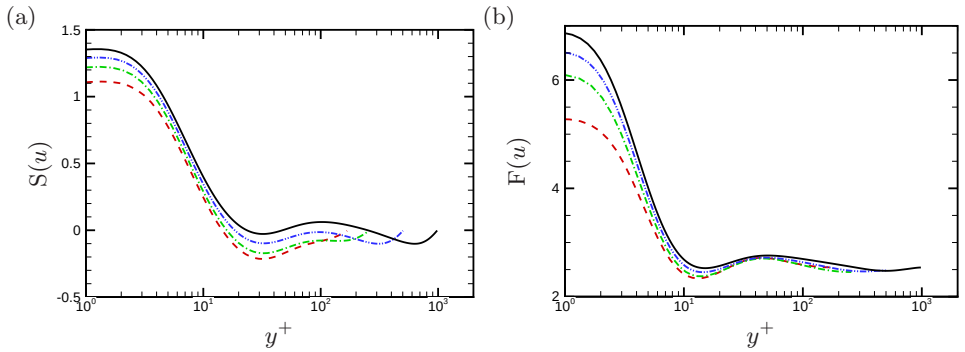

Figure 10: Skewness (a-b) and flatness (c-d) of streamwise velocity fluctuations. See table 1 for nomenclature of the DNS data.

turbulence kinetic energy is transferred toward the channel core and to the underlying layers, mainly because of the action of turbulent diffusion, and indeed we have verified that the contributions of pressure and viscous diffusion are negligible. This observation points to the activation of top-down mechanisms of influence of wall-distant eddies on the near-wall ones, in addition to the conventional bottom-up scenario (Hunt & Morrison 2001).

The presence of a top-down mechanism of influence is further evident in the streamwise velocity skewness and flatness maps, shown in figure 10. An increasing trend of both indicators is observed in the near-wall region, which suggests a more strongly intermittent character of the velocity signal. The increased near-wall intermittency in wall-bounded flows has been related (Mathis *et al.* 2009) to the modulation imparted by large-scale outer structures. In particular (Pirozzoli *et al.* 2011), it has been shown that in Couette flow large-scale high-speed events are connected to increased near-wall small-scale activity (and vice-versa), mainly because of locally increased wall friction. More quantitatively Schlatter & Örlü (2010) have shown that the local skewness of the streamwise velocity fluctuations is strongly correlated with the one-point amplitude modulation coefficient.

3.3. *Large-scale motions*

A visual impression of the large-scale eddies which form in the channel core is provided in figure 11(a), where we show streamwise velocity fluctuation contours in the channel symmetry plane ($\eta = 0$). A distinctive organization into h-scaled high- and low-speed streaks is evident, which maintain some coherence along the whole length of the channel, while also showing some meandering. The same type of representation is used for a cross-stream plane in figure 11(b), which shows that the core flow is mainly organized into 'towering' eddies which are attached to the walls, and which reach out to the opposite wall. Large-scale coherence is made clearer by averaging the flow fields in the streamwise direction, thus effectively filtering out small-scale fluctuations, as well as the streaks meandering (Papavassiliou & Hanratty 1997). In figure 11(c),(d) we show contours of the streamwise-averaged velocity fluctuations ($\tilde{u}$), and of the averaged streamwise vorticity ($\tilde{\omega}_x$), respectively. A clearer pattern emerges, with streaks having width of about 5h and occupying the whole channel thickness, and associated rollers, which show up in the form of alternating positive/negative streamwise vorticity zones. This pattern has been the subject of several previous studies (Waleffe 1997; Papavassiliou & Hanratty 1997; Tsukahara *et al.* 2006; Hwang & Cossu 2010), at much lower Reynolds number.

The quantitative effect of the core-flow rollers is considered next, by taking statistics of the velocity fluctuations associated with the streamwise-averaged fields. The resulting

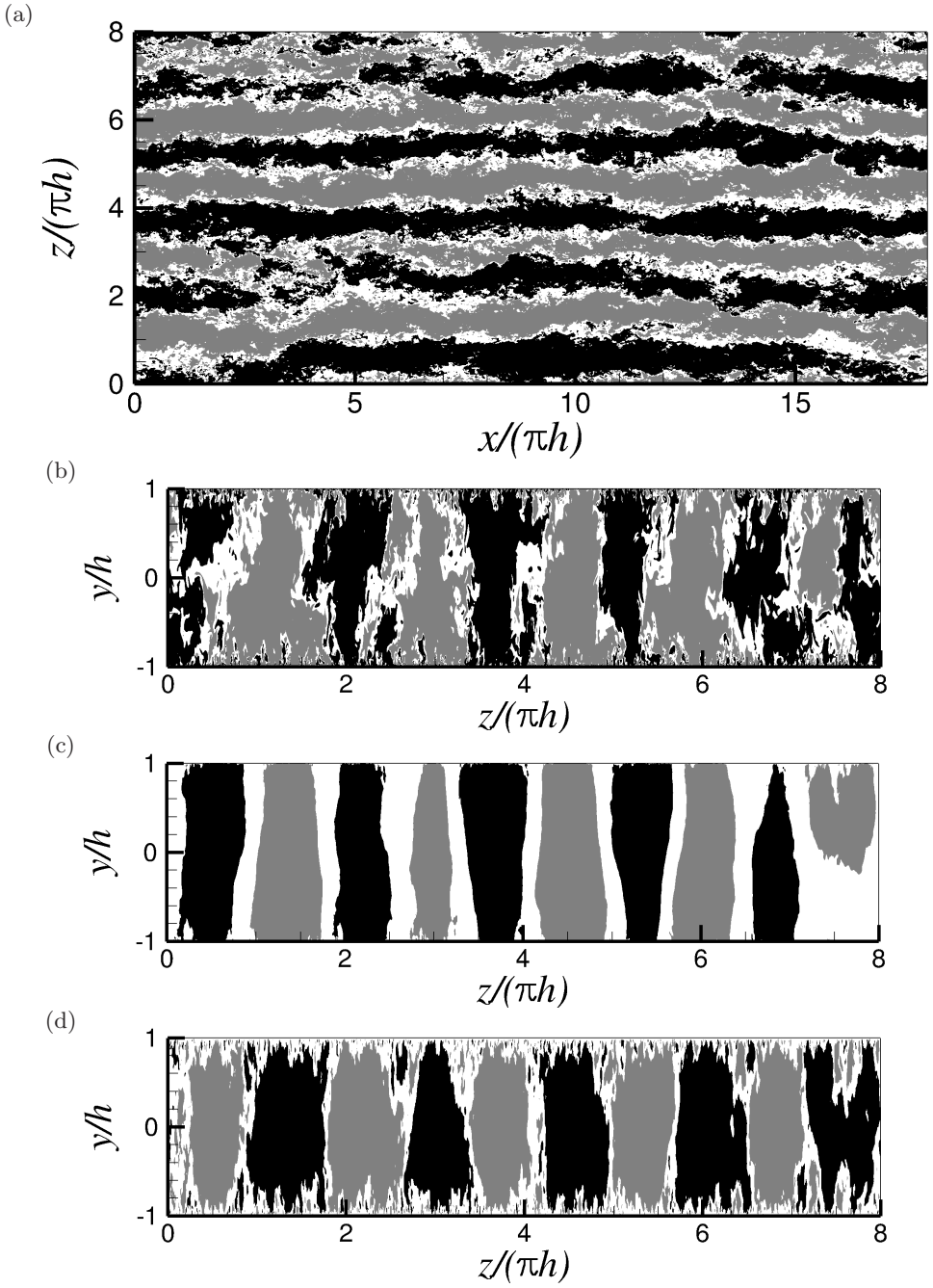

Figure 11: Visualization of instantaneous streamwise velocity in the channel centerplane (a) and in a cross-stream plane (b). Streamwise averages of u and of streamwise vorticity ω_x are given in frames (c) and (d). Note that axes in panels a-c are not to scale. Contour levels of u below $-u_\tau$ are shown in black, and contour levels above u_τ are shown in grey. Contour levels of ω_x below $-u_\tau/h$ are shown in black, and contour levels above u_τ/h are shown in grey.

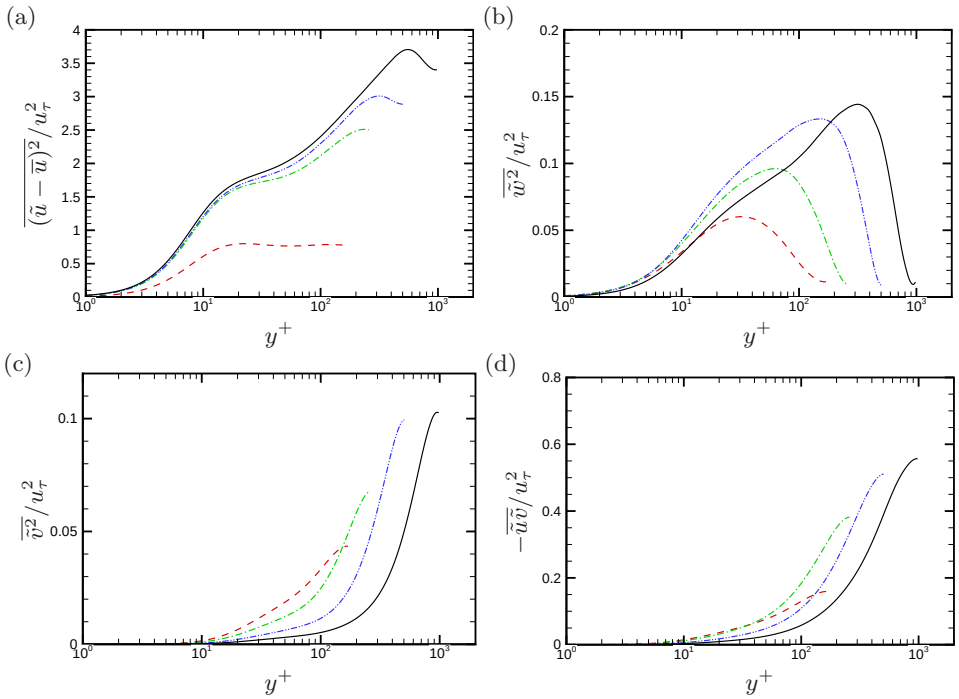

Figure 12: Distribution of coherent Reynolds stress components. The tilde symbol denotes instantaneous averaging in the streamwise direction. See table 1 for nomenclature of the DNS data.

'coherent-stress' components are shown in figure 12. The coherent part of the streamwise velocity variance is found to grow toward the channel centerline, attaining a peak at a distance $y/h \approx 0.4$ for flow cases C3, C4, which one can tentatively connect with the secondary peak of the streamwise Reynolds stress observed in figure 6. Its magnitude is found to account for about 50% of the overall velocity variance in the core part of the flow. Similar reasonings apply to the coherent turbulent shear stress, which if found to peak at the channel centerline, and which accounts for about half of the total shear stress. On the other hand, the rollers are found to contain little wall-normal and spanwise velocity fluctuations, probably because the v- and w-bearing eddies are less coherent in the streamwise direction, and undergo cancellation because of the averaging procedure. All the coherent stresses appear to increase with Re_τ when expressed in wall units, thus indicating increased importance of the core mode in the global dynamics.

4. Conclusions

Flow statistics from DNS of turbulent Couette flow at computationally high Reynolds number have been presented, in a range of Re_τ which well exceeds previous datasets. At $Re_\tau \gtrsim 500$ effects which are believed to be typical of the asymptotic high-Re regime start to manifest themselves. Visual fit of the mean velocity profiles suggests the formation of a range with near logarithmic behavior of the mean velocity, which is compatible with the classical set of coefficients, namely $k = 0.41$, $C = 5$. This fit is also adequate for practical purposes, in that the skin friction data are consistent with the classical logarithmic friction law, with zero value of the outer-layer constant. However, close inspection of the

log-law indicator function shows, rather than a plateau, significant excursions between two extrema, which become more severe as Re_τ is increased. Hence, extrapolation of the present data would suggest that a genuine log layer is not going to be found in Couette flow, even at extreme Reynolds number. This is in contrast with recent data for Poiseuille flow, which supports convergence to the logarithmic law, although only in the infinite Reynolds number limit. Data at yet higher Re_τ are certainly welcome to further verify this trend. The core velocity profile is found to be linear over a narrow interval across the centerline, and its minimum slope is found to slowly decrease in wall units. This is a strong hint that the asymptotic state of turbulent Couette flow consists of a flat velocity profile with finite slip at the two walls. Similar to other wall-bounded flows, the wall-parallel velocity variances exhibit a near-wall peak which seems to diverge logarithmically with Re_τ, and connected in the classical scenario with Townsend's attached eddies.

Notably, a secondary outer peak of the streamise velocity variance is observed in the highest Re simulation, which has not been observed so far in DNS of other canonical wall-bounded flows. This outer peak if found to occur at $y/h \approx 0.3$, and to well match the position of the outer site at which turbulence kinetic energy production exceeds dissipation. From a structural viewpoint, the emergence of excess energy in the outer layer has been traced to the presence of rollers/streaks which occupy the whole channel, and whose spectral signature consists of a sharp peak at a wavelength of about five channel half-heights. Conditional statistics have shown that these large eddies are responsible for a substantial fraction of the streamwise Reynolds stress, hence contributing to the formation of the outer peak of u', and to account for about a half of the turbulent shear stress in the channel core. Hence, they are likely to be responsible for the observed deviations of the mean velocity profile from a genuine logarithmic behavior. A side consequence of our observations is that, given the nearly sinusoidal behavior of the rollers in the spanwise direction, their correlation length scale is nominally infinite. Hence, data from both DNS and experiments of Couette flow are likely to be always contaminated by side effects, which would explain the large scatter observed in the existing literature, even for very basic flow properties.

Given this caveat, we believe that the present findings reinforce the statements made in Pirozzoli *et al.* (2011), that Couette flow can be regarded as an extreme state of wall turbulence, which can be used to explore with clarity phenomena of imprinting and modulation, without necessarily reverting to extreme-Reynolds-number simulations.

We acknowledge that some of the results reported in this paper have been achieved using the PRACE Research Infrastructure resource FERMI based at CINECA, Casalecchio di Reno, Italy.

REFERENCES

del Álamo, J. C., Jiménez, J., Zandonade, P. & Moser, R. D. 2004 Scaling of the energy spectra of turbulent channels. *J. Fluid Mech.* **500**, 135–144.

Alfredsson, P.H., Örlü, R. & Segalini, A. 2012 A new formulation for the streamwise turbulence intensity distribution in wall-bounded turbulent flows. *Europ. J. Mech.-B/Fluids* **36**, 167–175.

Alfredsson, P.H., Segalini, A. & Örlü, R. 2011 A new scaling for the streamwise turbulence intensity in wall-bounded turbulent flows and what it tells us about the 'outer' peak. *Phys. Fluids* **23**, 041702.

Avsarkisov, V., Hoyas, S., Oberlack, M. & García-Galache, J.P. 2014 Turbulent plane Couette flow at moderately high Reynolds number. *J. Fluid Mech.* **751**, R1.

Aydin, E.M. & Leutheusser, H.J. 1991 Plane-Couette flow between smooth and rough walls. *Exp. Fluids* **11**, 302–312.

Bech, K.H., Tillmark, N., Alfredsson, P.H. & Andersson, H.I. 1995 An investigation of turbulent plane Couette flow at low Reynolds numbers. *J. Fluid Mech.* **286**, 291–325.

Bernardini, M, Pirozzoli, S & Orlandi, P 2014 Velocity statistics in turbulent channel flow up to $\mathrm{Re}_\tau = 4000$. *J. Fluid Mech.* **742**, 171–191.

Bernardini, M, Pirozzoli, S, Quadrio, M & Orlandi, P 2013 Turbulent channel flow simulations in convecting reference frames. *J. Comput. Phys.* **232**, 1–6.

Busse, F.H. 1970 Bounds for turbulent shear flow. *J. Fluid Mech.* **41**, 219–240.

El Telbany, M. M. M. & Reynolds, A. J. 1982 Velocity distributions in plane turbulent channel flows. *Trans. ASME: J. Fluids Engng.* **104**, 367–372.

Hamilton, J. M., Kim, J. & Waleffe, F. 1995 Regeneration mechanisms of near-wall turbulent structures. *J. Fluid Mech.* **287**, 317348.

Hoyas, S. & Jiménez, J. 2006 Scaling of velocity fluctuations in turbulent channels up to $Re_\tau = 2003$. *Phys. Fluids* **18**, 011702.

Hoyas, S. & Jiménez, J. 2008 Reynolds number effects on the Reynolds-stress budgets in turbulent channels. *Phys. Fluids* **20**, 101511.

Hultmark, M., Vallikivi, M., Bailey, S.C.C. & Smits, A.J. 2012 Turbulent pipe flow at extreme Reynolds numbers. *Phys. Rev. Lett.* **108**, 094501.

Hunt, J.C.R. & Morrison, J.F. 2001 Eddy structure in turbulent boundary layers. *Eur. J. Mech. B Fluids* **19**, 673–694.

Hutchins, N. & Marusic, I. 2007 Evidence of very long meandering features in the logarithmic region of turbulent boundary layers. *J. Fluid Mech.* **579**, 1–28.

Hwang, Y. & Cossu, C. 2010 Amplification of coherent streaks in the turbulent Couette flow: an input-output analysis at low Reynolds number. *J. Fluid Mech.* **643**, 333–348.

Kim, J. & Moin, P. 1985 Application of a fractional-step method to incompressible Navier-Stokes equations. *J. Comput. Phys.* **59**, 308–323.

Kim, K.C. & Adrian, R.J. 1999 Very large-scale motion in the outer layer. *Phys. Fluids* **11**, 417–422.

Kitoh, O., Nakabayashi, K. & Nishimura, F. 2005 Experimental study on mean velocity and turbulence characteristics of plane Couette flow: low-Reynolds-number effects and large longitudinal vortical structure. *J. Fluid Mech.* **539**, 199–227.

Kitoh, O. & Umeki, M. 2008 Experimental study on large-scale streak structure in the core region of turbulent plane Couette flow. *Phys. Fluids* **20**, 025107.

Komminaho, J., Lundbladh, A. & Johansson, A.V. 1996 Very large structures in plane turbulent Couette flow. *J. Fluid Mech.* **320**, 259–285.

Lee, M.J. & Kim, J. 1991 The structure of turbulence in a simulated plane Couette flow. pp. 5.3.1–5.3.6. Munich: Proc. 8th Symp. Turbulent Shear Flows.

Mathis, R., Hutchins, N. & Marusic, I. 2009 Large-scale amplitude modulation of the small-scale structures in turbulent boundary layers. *J. Fluid Mech.* **628**, 311–337.

Metzger, M.M. & Klewicki, J.C. 2001 A comparative study of near-wall turbulence in high and low Reynolds number boundary layers. *Phys. Fluids* **13**, 692–701.

Monty, J.P., Hutchins, N., Ng, H.C.H., Marusic, I. & Chong, M.S. 2009 A comparison of turbulent pipe, channel and boundary layer flows. *J. Fluid Mech.* **632**, 431–442.

Orlandi, P. 2000 *Fluid fow phenomena: a numerical toolkit*. Kluwer.

Papavassiliou, D.V. & Hanratty, T.J. 1997 Interpretation of large-scale structures observed in a turbulent planet Couette flow. *Int. J. Heat Fluid Flow* **18**, 55–69.

Pirozzoli, S., Bernardini, M. & Orlandi, P. 2011 Large-scale organization and inner-outer layer interactions in turbulent Couette-Poiseuille flows. *J. Fluid Mech.* **680**, 534-563.

Pope, S.B. 2000 *Turbulent flows*. Cambridge University Press.

Reichardt, H. 1956 Über die Geschwindigkeitsverteilung in einer geradlinigen turbulenten Couetteströmung. *Z. Angew. Math. Mech.* **36**, 26–29.

Robertson, J.M. 1959 On turbulent plane Couette flow. In *Proc. Sixth Midwestern Conf. on Fluid Mechanics*, pp. 169–182. Univ. of Texas, Austin.

Schlatter, P. & Örlü, R. 2010 Quantifying the interaction between large and small scales in wall-bounded turbulent flows: a note of caution. *Phys. Fluids* **22**, 051704.

Schlichting, H. & Gersten, K. 2000 *Boundary layer theory*. 8th edn. Springer-Verlag.

Tillmark, N. & Alfredsson, P.H. 1992 Experiments on transition in plane Couette flow. *J. Fluid Mech.* **235**, 89–102.

Tillmark, N. & Alfredsson, P.H. 1998 Large scale structures in turbulent plane Couette flow pp. 59–62.

Townsend, A.A. 1976 *The Structure of Turbulent Shear Flow*. 2nd edn. Cambridge University Press.

Tsukahara, T., Kawamura, H. & Shingai, K. 2006 DNS of turbulent Couette flow with emphasis on the large-scale structure in the core region. *J. Turbul.* **7**, 1–16.

Waleffe, F. 1997 On a self-sustaining process in shear flows. *Phys. Fluids* **9**, 883–900.